Homogenization attempt of a wire-reiforced geomaterial

Romain Laniel* — **Pierre Alart*** — **Stéphane Pagano***

* *Laboratoire de Mécanique et Génie Civil*
UMR CNRS 5508, Université de Montpellier II
CC 048 Place Eugène Bataillon
34095 Montpellier cedex 5
laniel@lmgc.univ-montp2.fr

RÉSUMÉ. *Le mélange fil - sable possède de meilleurs propriétés mécaniques que le sable seul. Afin de mieux cerner les mécanismes de ce géo-composite, nous l'avons modélisé par des méthodes continues et discrètes. La formulation d'une loi thermodynamiquement admissible tenant compte de l'unilatéralité du renfort permet, en outre, une modélisation cohérente du matériau. Parallèlement, les investigations éléments discrets permettent de mettre en évidence les microphénomènes de renfort. Ce sont ces deux approches numériques que nous souhaitons confronter afin d'identifier les paramètres de notre loi continue.*

ABSTRACT. *The sand and wire mixture have a higher strength than the sand alone. We modeled it by continuous and discrete methods to emphasize its reinforcement mechanisms. In one hand, the formulation of a thermodynamics law which take into account for the wire network unilaterality, models consistently this material. In the other hand, investigations by discrete elements highlight reinforcement micro phenomena. We want to use these two numerical approaches to identify the parameters of our continuous law.*

MOTS-CLÉS : *Unilatéralité de la structure, thermodynamique, modélisation continue, modélisation discrète.*

KEYWORDS: *Structure unilaterality, thermodynamics, continuum modelling, discrete modelling.*

1. Motivations

Civil engineers are often expected to build larger and larger constructions ; the ground needs assistance in supporting such works. Various solutions can be used to reinforce soil, columns, micro-piles, geomembranes, geogrids and geotextiles. This paper focuses on a particular process, belonging to the last reinforcement category : *TexSol*™. It is a soil reinforcement process created in 1984 by Leflaive, Khay and Blivet from the LCPC (Laboratoire Central des Ponts et Chaussées) (Leflaive *et al.*, 1985) and (Khay *et al.*, 1990). Its originality lies in combining the soil (sand) with wires. A machine, called a "texsoleuse", does this by depositing sand and feeding in the wire at the same time. The latter is randomly distributed on the free surface and is simultaneously covered with sand to create a *TexSol*™ layer. Although the wire volume is

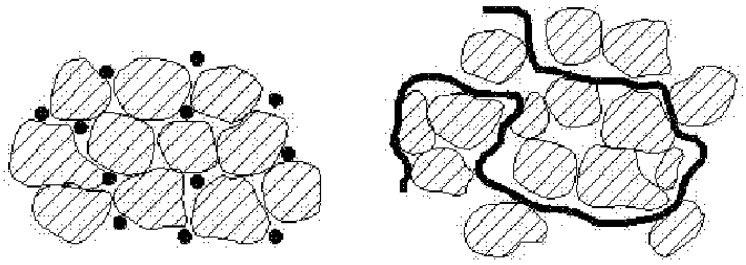

Figure 1. *Schematic TexSol*™ *sections*

negligible compared to that of the sand, the wire becomes a strong reinforcement when it tangles up inside the geomaterial (cf. Figure 1). The *TexSol*™ behavior depends on sand and wire constitutive parameters. They lead this mixed material friction angle to be larger than sand by 0° to 10° (Khay *et al.*, 1990). The wire is described by its linear density in dtex units ($1 \text{ dtex} = 10^{-7} \text{ kg.m}^{-1}$), ponderal content and stiffness. Classically, the wire density in a *TexSol*™ sample ranges between 10^5 m^{-2} and 3.10^5 m^{-2}. This type of material is adapted for embankments requiring a strong slope or works which may be subjected to dilatation strain (protection dome of a gas reserve for example). Indeed, the wire works in tensile directions and the wire network maintains the structure (when wire density is high enough) ; *TexSol*™ can be regarded as a composite material. In the literature, we find two different continuous modellings. The model suggested in (Fremond, 2002) is non local and includes remote interactions (corresponding to the wire effects) but requires identification of their parameters using macroscopic experiments. Villard proposes a simpler local model in (Villard *et al.*, 1989). It couples a standard model of sand and an equivalent unilateral elastic stiffness contribution corresponding to the wire network. This last contribution is activated only on the tension directions because of the unilateral behavior of wire. This study interest lies in multi-scale theoretical contributions of unilateral structures with long internal length. Thus, we propose to clearly define thermo-dynamical potentials

of the Villard local model with both stress and strain formulations to identify the best-adapted one. Such a stage is useful before carrying out a homogenization procedure applied to an untypical material. In the absence of physical experiments, the identification of macroscopic model will be performed using discrete numerical experiments. Those allow to study in detail the microstructure and reinforcement interactions on a microscopic scale.

2. Thermodynamical modelling in a local formalism

The local model proposed by Villard couples a standard model of sand with an equivalent unilateral elastic stiffness for the wire network. The unilateral characteristic of this feature means that stiffness is only activated in tensile directions. To "superpose" the elasto-plastic model of the sand and the unilateral elastic model of the wire network, some mechanical assumptions have to be considered : the strain rates equalities $\dot{\boldsymbol{\varepsilon}}_s = \dot{\boldsymbol{\varepsilon}}_w = \dot{\boldsymbol{\varepsilon}}$ and the stress additivity $\boldsymbol{\sigma} = \boldsymbol{\sigma}_s + \boldsymbol{\sigma}_w$. Those two assumptions

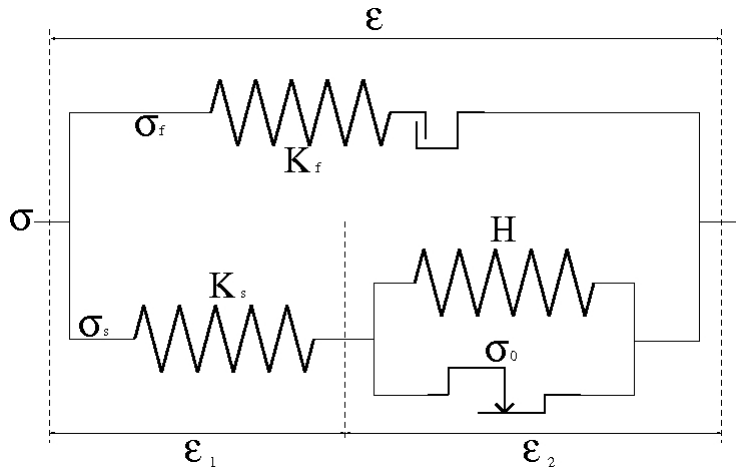

Figure 2. *Rheological TexSol™ diagram*

on the two phases are quiet restrictives and they would have to be verified by discrete simulations before carrying out an identification procedure. Figure 2 represents the mono-dimensional rheological diagram of both sand and wire network model, superposed using the two previous assumptions. We want to write this type of model in a consistent thermodynamical framework with both strain and stress formulations. The interest of this work lies in the identification possibilities of thermodynamical potentials parameters.

2.1. *Several descriptions of a thermodynamics state*

We thus use the Legendre–Fenchel transformation, to carry out our study with both strain and stress formulations. Let us write the Clausius–Duhem inequality where u is the internal energy, s the massic entropy, q the heat flow vector and T the temperature,

$$\boldsymbol{\sigma} : \dot{\boldsymbol{\varepsilon}} - \rho \left(\dot{u} - T\dot{s} \right) - \frac{q}{T} \cdot \nabla T \geq 0 \, . \qquad [1]$$

The intrinsic dissipation depends on a state variable $\boldsymbol{X}$ (or its dual $\boldsymbol{X}^*$), some internal variables $\alpha = \{\alpha_1, \cdots, \alpha_p\}$ (each internal variable can be scalar, vectorial or tensorial) and the temperature T. It can also be expressed with the free energy $\psi = u - Ts$ or its Legendre–Fenchel transformation ψ^* with respect to the state variable $\boldsymbol{X}$,

$$\begin{cases} \psi(\boldsymbol{X}, \alpha, T) = u(\boldsymbol{X}, \alpha, T) - Ts(\boldsymbol{X}, \alpha, T) \\ \psi^*(\boldsymbol{X}^*, \alpha, T) = \sup\limits_{\overline{\boldsymbol{X}}} \left\{ \overline{\boldsymbol{X}} \ : \boldsymbol{X}^* - \psi(\overline{\boldsymbol{X}}, \alpha, T) \right\} \\ \qquad\qquad\quad = \boldsymbol{X} \ : \boldsymbol{X}^* - \psi(\boldsymbol{X}, \alpha, T) \, . \end{cases} \qquad [2]$$

where $\boldsymbol{X}$ is the argument of the supremum. Considering either $\boldsymbol{X}$ or $\boldsymbol{X}^*$, we find two expressions of the Clausius–Duhem inequality,

$$\boldsymbol{\sigma} \ : \dot{\boldsymbol{\varepsilon}} - \rho \left[\tfrac{\partial \psi}{\partial \boldsymbol{X}} \ : \dot{\boldsymbol{X}} + \left(s + \tfrac{\partial \psi}{\partial T} \right) \dot{T} + \tfrac{\partial \psi}{\partial \alpha_m} \dot{\alpha}_m \right] - \tfrac{q}{T} \cdot \nabla T \geq 0 \quad , \qquad [3]$$

$$\boldsymbol{\sigma} \ : \dot{\boldsymbol{\varepsilon}} - \rho \left[\dot{\boldsymbol{X}} \ : \boldsymbol{X}^* + \left(\boldsymbol{X} - \tfrac{\partial \psi^*}{\partial \boldsymbol{X}^*} \right) \ : \dot{\boldsymbol{X}}^* + \left(s - \tfrac{\partial \psi^*}{\partial T} \right) \dot{T} - \tfrac{\partial \psi^*}{\partial \alpha_m} \dot{\alpha}_m \right] - \tfrac{q}{T} \cdot \nabla T \geq 0 \, . \qquad [4]$$

Using the Helmholtz postulate, we deduce one part of the state laws, and we also define thermodynamical forces $\mathcal{A}_m$ associated to internal variables α_m to complete those laws such as,

Primal state laws	*Dual state laws*
$\boldsymbol{X}^* \in \partial_{\boldsymbol{X}} \psi(\boldsymbol{X}, \alpha, T)$	$\boldsymbol{X} \in \partial_{\boldsymbol{X}^*} \psi^*(\boldsymbol{X}^*, \alpha, T)$
$-s \in \partial_T \psi(\boldsymbol{X}, \alpha, T)$	$s \in \partial_T \psi^*(\boldsymbol{X}^*, \alpha, T)$
$-\frac{\mathcal{A}_m}{\rho} \in \partial_{\alpha_m} \psi(\boldsymbol{X}, \alpha, T)$	$\frac{\mathcal{A}_m}{\rho} \in \partial_{\alpha_m} \psi^*(\boldsymbol{X}^*, \alpha, T)$

[5]

Formally, we use subdifferentials instead of derivatives. In the general case, the Clausius–Duhem inequality (3) or (4) can be reduced to a dot product of a vector flow and a vector force. It is convenient to introduce a dissipation potential φ from which the evolution laws are derived. By duality, a force function φ^* is automatically defined using the Legendre–Fenchel transformation. Generally, we distinguish the reversible and irreversible parts of the transformation. We thus postulate an additive decomposition for both reversible and irreversible parts of the strain tensor $\boldsymbol{\varepsilon} = \boldsymbol{\varepsilon}^{\mathrm{r}} + \boldsymbol{\varepsilon}^{\mathrm{ir}}$ and the

State variable : $\boldsymbol{\varepsilon}^{\mathrm{r}}$		***State variable : $\boldsymbol{\sigma}$***	
$\boldsymbol{\sigma} : \dot{\boldsymbol{\varepsilon}}^{\mathrm{ir}} + \mathcal{A}_m \dot{\alpha}_m - \frac{q}{T} \cdot \nabla T \geq 0$		$\boldsymbol{\sigma} : \dot{\boldsymbol{\varepsilon}}^{\mathrm{ir}} + \mathcal{A}_m \dot{\alpha}_m - \frac{q}{T} \cdot \nabla T \geq 0$	
Free energy : ψ	Dissipation potential : φ	Free enthalpy : ψ^*	Force function : φ^*
$\frac{1}{\rho}\boldsymbol{\sigma} \in \partial_{\boldsymbol{\varepsilon}^{\mathrm{r}}} \psi$ $-s \in \partial_T \psi$ $-\frac{1}{\rho}\mathcal{A}_m \in \partial_{\alpha_m} \psi$	$\boldsymbol{\sigma} \in \partial_{\dot{\boldsymbol{\varepsilon}}^{\mathrm{ir}}} \varphi$ $\mathcal{A}_m \in \partial_{\dot{\alpha}_m} \varphi$ $\nabla T \in \partial_{\left(-\frac{q}{T}\right)} \varphi$	$\frac{1}{\rho}\boldsymbol{\varepsilon}^{\mathrm{r}} \in \partial_{\boldsymbol{\sigma}} \psi^*$ $s \in \partial_T \psi^*$ $\frac{1}{\rho}\mathcal{A}_m \in \partial_{\alpha_m} \psi^*$	$\dot{\boldsymbol{\varepsilon}}^{\mathrm{ir}} \in \partial_{\boldsymbol{\sigma}} \varphi^*$ $-\mathcal{A}_m \in \partial_{\dot{\alpha}_m} \varphi^*$ $-\nabla T \in \partial_{\left(-\frac{q}{T}\right)} \varphi^*$
State variable : $\boldsymbol{\varepsilon}$		***State variable : $\boldsymbol{\sigma}^{\mathrm{r}}$***	
$\boldsymbol{\sigma}^{\mathrm{ir}} : \dot{\boldsymbol{\varepsilon}} + \mathcal{A}_m \dot{\alpha}_m - \frac{q}{T} \cdot \nabla T \geq 0$		$\boldsymbol{\sigma}^{\mathrm{ir}} : \dot{\boldsymbol{\varepsilon}} + \mathcal{A}_m \dot{\alpha}_m - \frac{q}{T} \cdot \nabla T \geq 0$	
Free energy : ψ	Dissipation potential : φ	Free enthalpy : ψ^*	Force function : φ^*
$\frac{1}{\rho}\boldsymbol{\sigma}^{\mathrm{r}} \in \partial_{\boldsymbol{\varepsilon}} \psi$ $-s \in \partial_T \psi$ $-\frac{1}{\rho}\mathcal{A}_m \in \partial_{\alpha_m} \psi$	$\boldsymbol{\sigma}^{\mathrm{ir}} \in \partial_{\dot{\boldsymbol{\varepsilon}}} \varphi$ $\mathcal{A}_m \in \partial_{\dot{\alpha}_m} \varphi$ $\nabla T \in \partial_{\left(-\frac{q}{T}\right)} \varphi$	$\frac{1}{\rho}\boldsymbol{\varepsilon} \in \partial_{\boldsymbol{\sigma}^{\mathrm{r}}} \psi^*$ $s \in \partial_T \psi^*$ $\frac{1}{\rho}\mathcal{A}_m \in \partial_{\alpha_m} \psi^*$	$\dot{\boldsymbol{\varepsilon}} \in \partial_{\boldsymbol{\sigma}^{\mathrm{ir}}} \varphi^*$ $-\mathcal{A}_m \in \partial_{\dot{\alpha}_m} \varphi^*$ $-\nabla T \in \partial_{\left(-\frac{q}{T}\right)} \varphi^*$

Tableau 1. *Strain versus stress formulations*

stress tensor $\boldsymbol{\sigma} = \boldsymbol{\sigma}^{\mathrm{r}} + \boldsymbol{\sigma}^{\mathrm{ir}}$. At this stage, we have to choose the external state variable $\boldsymbol{X}$ for the strain formulation and consequently $\boldsymbol{X}^*$ for the stress formulation. The two most relevant choices are given in Table 1. Classically, an experimenter choose an observable variable as the total strain $\boldsymbol{\varepsilon}$, but other variables can be used as the reversible strain $\boldsymbol{\varepsilon}^{\mathrm{ir}}$. This choice changes dual variables, state and complementary laws and the inequality (1).

2.2. *Thermodynamical potentials of the TexSol™ in a three-dimensional modelling*

Concerning our continuous model, the sand phase is described by an elastic-plastic model with an isotropic and kinematic hardening combination. The sand elastic domain is bounded by a Drucker – Prager criterion which is regular and close enough from the classic soil criterion of Mohr – Coulomb. We consider that the wire network phase behave like an elastic three-dimensional structure when it is fully in tension. However, the continuous law have to take into account the unilateral characteristic of a wire element at the structure scale. Those two phase model are superposed by the strain rates equality and the stress additivity as mentioned in section 2. We choose $\boldsymbol{\varepsilon}$ as the state variable combined with the internal variables $\boldsymbol{\varepsilon}^{\mathrm{p}}$, $\boldsymbol{\alpha}$ and p describing the plasticity, kinematic and isotropic hardening respectively. The model elastic parameters are the sand elasticity tensor $\mathbb{K}_s$, depending on the sand elasticity modulus E_s and ν_s, and the wire network coefficients of Lamé λ_w and μ_w. The hardening ones are H_i and H_k the isotropic and kinematic hardening respectively. The *TexSol*™ free energy is written as,

$$\begin{aligned}
&\psi(\boldsymbol{\varepsilon}, \boldsymbol{\varepsilon}^{\mathrm{p}}, \boldsymbol{\alpha}, p) = \psi_s(\boldsymbol{\varepsilon}, \boldsymbol{\varepsilon}^{\mathrm{p}}, \boldsymbol{\alpha}, p) + \psi_w(\boldsymbol{\varepsilon}) \\
&\psi_s(\boldsymbol{\varepsilon}, \boldsymbol{\varepsilon}^{\mathrm{p}}, \boldsymbol{\alpha}, p) = \tfrac{1}{2}\left(\boldsymbol{\varepsilon} - \boldsymbol{\varepsilon}^{\mathrm{p}}\right) : \mathbb{K}_s \left(\boldsymbol{\varepsilon} - \boldsymbol{\varepsilon}^{\mathrm{p}}\right) + \tfrac{H_{\mathrm{k}}}{2}\boldsymbol{\alpha} : \boldsymbol{\alpha} + \tfrac{H_{\mathrm{i}}}{2} p^2 \\
&\psi_w(\boldsymbol{\varepsilon}) = \tfrac{\lambda_w}{2}\langle \mathrm{tr}(\boldsymbol{\varepsilon}) \rangle^2 + \mu_w \boldsymbol{\varepsilon}^{\geq} : \boldsymbol{\varepsilon}^{\geq} ,
\end{aligned} \qquad [6]$$

where $\langle . \rangle = \max(., 0)$. The spheric term of the wire network free energy has regard of the unilaterality of the volumic deformation. Concerning the other one, it has to activate the wire stiffness only on the tensile principle directions. The operator $(.^{\geq})$, described more precisely in (Laniel *et al.*, 2007), is define by $\boldsymbol{\varepsilon}^{\geq} = \boldsymbol{P}\langle \text{diag}(\varepsilon_1, \varepsilon_2, \varepsilon_3)\rangle \boldsymbol{P}^T$, where ε_1, ε_2, ε_3 and $\boldsymbol{P}$ are the principle values and the passage matrix of $\boldsymbol{\varepsilon}$ respectively. The wire network model is non dissipative, consequently the *TexSol*™ and the sand dissipation potentials are the same. We thus write the Legendre – Fenchel transform of the dissipation potential as,

$$\varphi^*(\boldsymbol{\sigma}^{ir}, \boldsymbol{A}, \boldsymbol{\chi}, R) = \mathrm{I}_{\{\mathbf{0}\}}(\boldsymbol{\sigma}_s^{ir}) + \mathrm{I}_{\Omega(\boldsymbol{\chi},R)}(\boldsymbol{A}) \,, \qquad [7]$$

where $\boldsymbol{\sigma}^{\text{ir}}$, $\boldsymbol{A}$, $\boldsymbol{\chi}$ and R are thermodynamical forces associated to $\boldsymbol{\varepsilon}$, $\boldsymbol{\varepsilon}^p$, $\boldsymbol{\alpha}$ and p respectively. The indicative function of a $\mathcal{D}$ domain is noted $\mathrm{I}_{\mathcal{D}}(.)$. In the principle stresses space, Ω represents the elastic domain which is bound by a Drucker – Prager criterion depending on the internal friction angle θ_f and the cohesion C_0, as mentioned previously. The state laws and complementary laws associated to potentials (6) and (7) have been implemented and tested in the finite element software *Cast3M*™. Three different models are tested : a sand alone called "sand", a sand bilaterally reinforced called "reinforced sand" and a sand unilaterally reinforced called "texsol". A

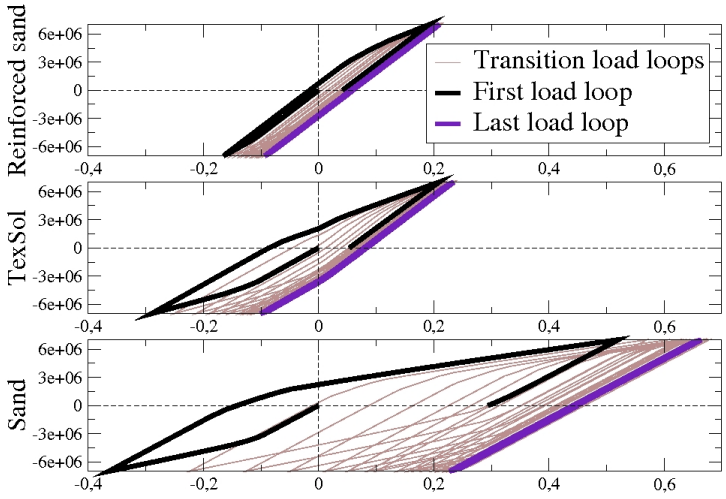

Figure 3. *Cyclic compression test*

cyclic compression test is carried out, using a single linear element and a piloted displacement, on the three models to emphasize the unilateral properties of the *TexSol*™ compared to the two other limit models. After 20 loading loops, we remark in Figure 3 that all force/displacement plots are stabilized. However, "texsol" and "reinforced sand" stabilization occurs earlier and closer to the zero displacement axis than "sand" one. We can also clearly observe a switch in the *TexSol*™ slope depending on the tension

or compression domain. Another test is carried out to highlight the repartition of the wire network stress. We thus simulate a crushing test of 0.1% on a cylinder meshed by 400 linear elements. Figure 5 shows the equivalent Von-Mises stress σ^{eq} map on a

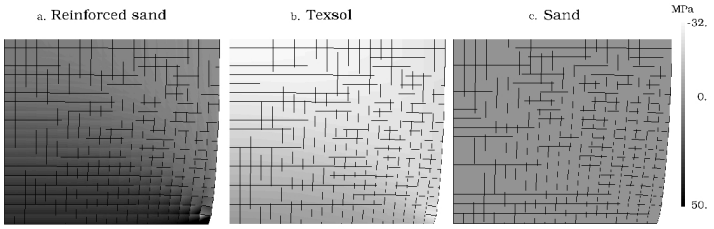

Figure 4. *Wire network pressure*

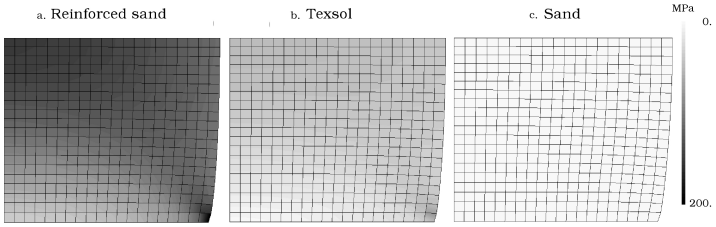

Figure 5. *Wire network equivalent stress*

axial/radial section of the sample ($\sigma^{\text{eq}} = \sqrt{J_2(\boldsymbol{S})}$ is considered as the pseudo norm of the deviatoric stress tensor $\boldsymbol{S}$). The wire network equivalent stress level of the "texsol" is bounded by the two other models but the repartition is close to that of "reinforced sand". The wire network pressure map is shown in the Figure 4 and we remark that the "texsol" generates only negative pressure in the wire network phase, due to its unilateral definition.

3. Numerical discrete investigations

It is classical to identify the material parameters (stiffness, hardening et cætera) in a continuous model of a complex structure, by carrying out a backward analysis. Experimental tests are generally used to update the set parameters but the measurable fields are limited (surface strain, partial displacement field, total force on boundary conditions). In our approach, the measure fields are replaced by discrete numerical experiments. Thus, all the particle displacements and contact forces can be extracted from the sample. By locally averaging the previous fields, the equivalent stress and strain tensors of the granular material are built up (Bagi, 1996),(Cambou *et al.*, 2001).

These provide more accurate information than the experimental method with a more relevant cost function.

3.1. *A discrete modelling of the TexSol™*

The NSCD is a discrete element method used in the *LMGC90* code which simulates multibody vs. multicontact problems, privileging velocity fields (Jean, 1999). For a single contact α problem, the NSCD evaluates the external forces and dynamic effects on the contactor point. To make such a transformation, $\boldsymbol{H}_\alpha$ and $\boldsymbol{H}_\alpha^T$ are used to move variables from the local contact frame to the global body and vice-versa. For a time step $i+1$, a linear relation between the relative velocity u_{i+1}^α and the averaged impulse p_{i+1}^α over $[t_i, t_{i+1}]$ is found ; this is associated to a contact condition such as,

$$\left\{ \begin{array}{l} u_{i+1}^\alpha - \boldsymbol{W}^{\alpha\alpha} p_{i+1}^\alpha = u_{\text{free},i}^\alpha + \sum_{\beta\neq\alpha} \boldsymbol{W}^{\alpha\beta} p_{i+1}^\beta \\ \text{Law}[u_{i+1}^\alpha, p_{i+1}^\alpha] = \text{true} \ . \end{array} \right. \quad [8]$$

The smooth dynamic effects are included in the expression of the relative free velocity $u_{\text{free},i}^\alpha$. The Delassus operator $\boldsymbol{W}^{\alpha\beta} = \boldsymbol{H}_\alpha^T \boldsymbol{M}^{-1} \boldsymbol{H}_\beta$ naturally appears in the dynamics reduced to contacts. In this way, for a frictionless problem with a Signorini contact condition $0 \leq u_{n,i+1} \perp p_{n,i+1} \geq 0$, the system (8) reveals to be a standard Linear Complementarity Problem (LCP). For a frictional contact problem, tangential reactions and tangential velocities have to verify a similar non smooth relation. A Gauss – Seidel loop computes all contact reactions until convergence.

In the *NSCD* framework, the wire network must be discretized. So, it is broken up into a collection of equidistant material points, with the wire mass equal to the sum of all point masses. All these points must be connected by a behavior law which accounts for a small segment of wire. The wire must keep its free flexion and unilaterality properties. Consequently, a wire contact law concerns only the normal direction and there is no constraint on the tangential directions. In all cases, flexion is imposed and mesoscopic unilaterality can be seen, as, in longitudinal compression, the discrete wire (more than two points) behaves like a buckling beam. Thus, four laws, supported by contactor *points*, can be introduced (cf. Figure 7) implemented in *LMGC90*, corresponding to four different wire behaviors :

– ***"Rigid rod"*** : this couples the normal velocity of both candidate and antagonist particles.

– ***"Elastic rod"*** : this law adds regularisation (due to elasticity k) to the contact problem in both compression and tensile directions.

– ***"Rigid wire"*** : this is a **unilateral** law which couples the normal velocity of both particles only if the element strain tend to be positive.

– ***"Elastic wire"*** : this includes unilaterality and the wire stiffness parameter k ; *"elastic rod"* and *"rigid wire"* are coupled into this interaction law.

An advantage of the "unilateral" laws is that the returned reaction on the contact element is only tensile, better accounting for the wire behavior. Finally, to ensure the

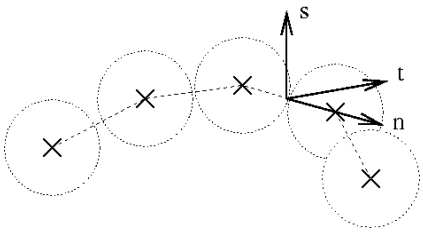

Figure 6. *Discrete wire modeled by a chain of beads with a local contact frame.*

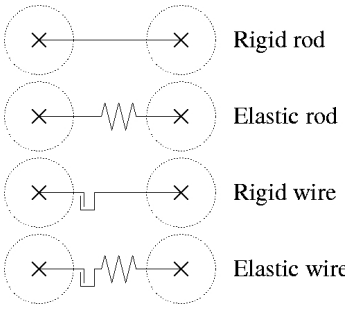

Figure 7. *Schematic representation of different wire interaction laws on the normal axis.*

interactions between the wire and the sand, *spheres* (as contactors) are attached to all material *points*. This allows the wire to be modeled by a chain of beads (cf. Fig. 6).

3.2. *Numerical experiments*

Once the *TexSol*™ sample clearly generates as a granular media (Radjaï *et al.*, 1998), mechanical tests can be carried out. Large vs. small strain tests are distinguished to emphasize the differences in reinforcement mechanisms. First a qualitative test on a *TexSol*™ slope highlights the reinforcement mechanisms often associated with this special material. This test consisted in depositing a geometrically densified sample on a rubber plan assimilated to a collection of equal radius beads in a hexagonal distribution. The initial sample includes a wire network, quasi-equiprobably distributed, discretized by beads which are connected with an *"elastic wire"* contact law. The simulation is carried out by *LMGC90* until sample kinetic energy is close to zero. Indeed the reinforcement structure was mobile and subsided following the sand particles. But this transformation leads the wire to form horizontal "stoppings" around the divergent particle flow which prevent sand circulation under gravity. The wire network becomes orthotropic. Consequently, the slope friction angle of the *TexSol*™ is higher than the sand one ; numerical and experimental values coincided (Khay *et al.*, 1990) lying between 0° to 10°.

The previous test dealt with reinforcement mechanisms in large transformations. But with a small strain background the wire network is not as mobile and may not generate long distance interactions as previously. Therefore, a triaxial test was carried out on a box-shaped sample. We also define a tool which is able to emphasize the interaction length inside a material (i.e. the *characteristic length* discriminating the local or non local behavior).

DEFINITION. *We call $\overline{\lambda}^m$ the length of a wire segment with a tension higher than mp_{avg}, where p_{avg} is the average tension of the wire network and $m \in \mathbb{R}^+$. Moreover we use the maximum length $\overline{\lambda}^m_{\text{max}}$ such as,*

$$\overline{\lambda}^m_{\text{max}} = \sup_{s_1,s_2} \left\{ \int_{s_1}^{s_2} ds \middle| \forall s \in [s_1, s_2] \text{ with } s_1, s_2 \in [0, L], |p(s)| \geq mp_{\text{avg}} \right\} ,$$

where s, s_1 and s_2 are curvilinear coordinates associated to the wire. It seems that $m = 3$ is a good compromise to vanish weak segments and to highlight strong segments.

We compare in Figure 8 the *characteristic length*, assimilated to $\overline{\lambda}^3_{\text{max}}$, of the two tests ; we also give in Table 2 the number of mid-ray particles of the granular media which is equal to this *characteristic length*. The test implying large transformations,

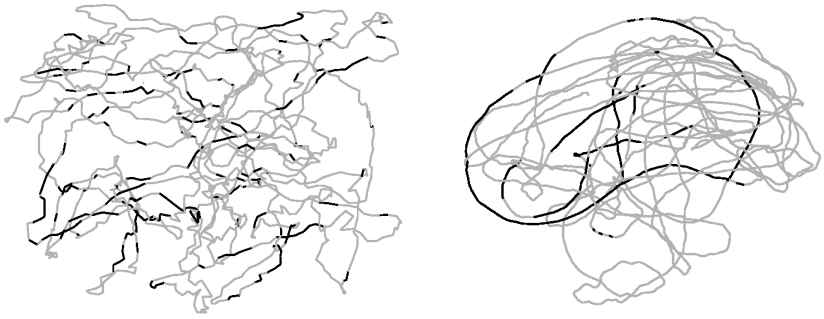

(a) Active wire segments after a triaxial test (b) Active wire segments in a deposit slope

Figure 8. *Active wire segments distributions for both small and large strain assumptions*

Tests	$\overline{\lambda}^3_{\text{max}}$	Equivalence number of mid-ray particles
Slope deposit	21.56 mm	54
Triaxial test	4.29 mm	4

Tableau 2. *Characteristic length comparison for different tests*

leads to changes of the reinforcement structure which tend to linearize itself. This transformation is not alleviating, since it supports the propagation of the tension and then increases the remote effects. Quiet contrary, the loading applied on triaxial test induces small strains which involve the reinforcement quasi-staticity and generate several small wire active elements. Consequently, this test is considered as a local one

and dimensions of a representative elementary volume of *TexSol*™ must be, at least, higher than the *characteristic length*. The parameters of the wire discrete model may also have an influence on reinforcement mechanisms, especially the diameter of the wire beads. We simulate triaxial tests where the wire beads diameter are decreasing and we observe that the average strains of both phases diverge when wire beads are too small. The related physical phenomenon is the sudden large sliding of the wire with respect to the sand. This sliding occurs in the same direction leading to a non symmetry of the two horizontal wire strains. The thinner the wire, the more it slips. These relative slidings conflict with the assumptions of the continuous model. Thus, if an identification approach is performed using discrete element investigations, the validity limits can be so defined.

4. *TexSol*™ behaviour and identification

During the triaxial process, the wire network stress level increases linearly as shown in Figure 9. The reinforcement is considered as a linear elastic structure for both “elastic” and “rigid” contact laws, which is surprising for the rigid network. The

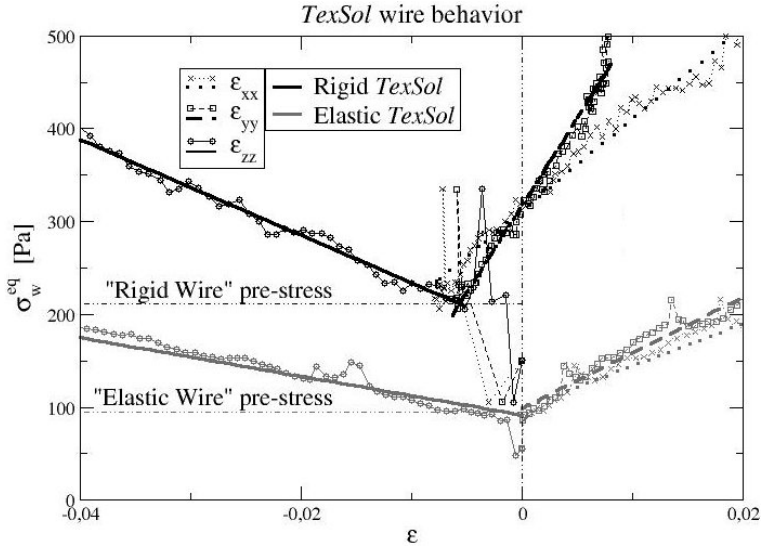

Figure 9. *Wire equivalent stress vs. strains plots for TexSol*™ *samples*

first has a stress shift due to the sample preparation above. This increase with wire stiffness but a strain shift appears, especially for the “rigid wire”. From the very start of the triaxial test, wire behavior is disturbed by a brutal contracting reorganization amplified for “rigid wire”. The slope of the $(\varepsilon_{zz}, \sigma_w^{\text{eq}})$ plot may represent a macro-stiffness. This one increases with the micro-stiffness k but not linearly. Indeed, it tends

to stabilize around a limit macro-stiffness corresponding to that of "rigid wire". Using average fields $\boldsymbol{\varepsilon}_s$, $\boldsymbol{\sigma}_s$, $\boldsymbol{\varepsilon}_w$ and $\boldsymbol{\varepsilon}_w$ of a homogeneous test (as triaxial), a global identification procedure of the continuous model is then carried out. It starts by identifying the elastic parameters E_s, E_w and $\nu_s = \nu_w$ (since we assume that $\boldsymbol{\varepsilon} = \boldsymbol{\varepsilon}_s = \boldsymbol{\varepsilon}_w$) from the previous fields in an elastic domain. Several tests, using different confinement pressures, are simulated to determine the Drucker – Prager criterion coefficients θ_f and C_0. Finally, we use a finite element method updating (FEMU), reduced to the hardening modulus H_{k} and H_{i}, to conclude the identification procedure. This identi-

Pression [bars]	E_w [kPa]	E_s [kPa]	τ_y [Pa]	H_{k} [kPa]	H_{i} [kPa]
0.5	405.4	11 302	6 832	800	400
0.6	321.4	12 280	6 947	1 000	500
0.7	305.1	9 701	8 429	1 040	520
0.8	309.5	14 606	9 679	960	480
0.9	318.7	12 948	5 810	920	460

Tableau 3. *Identification of elastic modulus E_s and E_w, shearing limit τ_y and hardening modulus H_{k} and H_{i}, with respect to the confinement pressure*

fication procedure of a given *TexSol*™ sample included in spherical domain (to limit edge effects) and subjected to a triaxial compression test, provides $\nu_s = \nu_w = 0.2$, $\theta_f = 0.079$ rad, $C_0 = 2\,842$ Pa and values given in Table 3. Those are constant with respect to the confinement pressure.

5. Bibliographie

Bagi K., « Stress and strain in granular assemblies », *Mechanics of materials*, n° 22, p. 165-177, 1996.

Cambou B., Jean M., *Micromécanique des matériaux granulaires*, Hermès, Science-Paris, 2001.

Fremond M., *Non-Smooth Thermo-mechanics*, Springer-Verlag, Berlin Heidelberg New York, 2002.

Jean M., « The non smooth contact dynamics method », *Computer Methods in Applied Mechanic and Engineering*, n° 177 (Special issue), p. 235-257, 1999.

Khay M., Gigan J.-P., TEXSOL - Ouvrage de soutènement, Technical report, LCPC, 1990.

Laniel R., Alart P., Pagano S., « Consistent thermodynamic modelling of wire-reinforced materials », *European Journal of Mechanics - A/Solids*, vol. 26, p. 854-871, 2007.

Leflaive E., Khay M., Blivet J.-C., « Un nouveau matériaux : le TEXSOL », *Travaux*, n° 602, p. 1-3, 1985.

Radjaï F., Wolf D. E., Jean M., Moreau J.-J., « Bimodal Character of Stress Transmission in Granular Packings », *Phys. Rev. Lett.*, vol. 80, n° 1, p. 61-64, 1998.

Villard P., Jouve P., « Behavior of granular materials reinforced by continuous threads », *Computers and Geothechnics*, vol. 7, p. 83-98, 1989.

ANNEXE POUR LE SERVICE FABRICATION
A FOURNIR PAR LES AUTEURS AVEC UN EXEMPLAIRE PAPIER
DE LEUR ARTICLE ET LE COPYRIGHT SIGNE PAR COURRIER
LE FICHIER PDF CORRESPONDANT SERA ENVOYE PAR E-MAIL

1. ARTICLE POUR LA REVUE :
L'objet. Volume ?? – n°??/2007

2. AUTEURS :
Romain Laniel[*] *— Pierre Alart*[*] *— Stéphane Pagano*[*]

3. TITRE DE L'ARTICLE :
Homogenization attempt of a wire-reiforced geomaterial

4. TITRE ABRÉGÉ POUR LE HAUT DE PAGE MOINS DE 40 SIGNES :
TexSol™ homogenization attempt

5. DATE DE CETTE VERSION :
29 septembre 2007

6. COORDONNÉES DES AUTEURS :

– adresse postale :
[*] Laboratoire de Mécanique et Génie Civil
UMR CNRS 5508, Université de Montpellier II
CC 048 Place Eugène Bataillon
34095 Montpellier cedex 5
laniel@lmgc.univ-montp2.fr
– téléphone : 04 67 14 45 37
– télécopie :
– e-mail : laniel@lmgc.univ-montp2.fr

7. LOGICIEL UTILISÉ POUR LA PRÉPARATION DE CET ARTICLE :
LaTeX, avec le fichier de style `article-hermes.cls`,
version 1.23 du 17/11/2005.

8. FORMULAIRE DE COPYRIGHT :
Retourner le formulaire de copyright signé par les auteurs, téléchargé sur :
`http://www.revuesonline.com`

SERVICE ÉDITORIAL – HERMES-LAVOISIER
14 rue de Provigny, F-94236 Cachan cedex
Tél. : 01-47-40-67-67
E-mail : revues@lavoisier.fr
Serveur web : http://www.revuesonline.com